Observation of non-Fermi liquid behavior in hole-doped $LiFe_{1-x}V_xAs$

L. Y. Xing,[1] X. Shi,[1] P. Richard,[1,2,3,*] X. C. Wang,[1,†] Q. Q. Liu,[1] B. Q. Lv,[1] J.-Z. Ma,[1] B. B. Fu,[1] L.-Y. Kong,[1] H. Miao,[4]
T. Qian,[1,2] T. K. Kim,[5] M. Hoesch,[5] H. Ding,[1,2,3,‡] and C. Q. Jin[1,2,3,§]

[1]*Beijing National Laboratory for Condensed Matter Physics, and Institute of Physics, Chinese Academy of Sciences, Beijing 100190, China*
[2]*Collaborative Innovation Center of Quantum Matter, Beijing, China*
[3]*School of Physical Sciences, University of Chinese Academy of Sciences, Beijing 100190, China*
[4]*Condensed Matter Physics and Materials Science Department, Brookhaven National Laboratory, Upton, New York 11973, USA*
[5]*Diamond Light Source, Harwell Campus, Didcot OX11 0DE, United Kingdom*

We synthesized a series of V-doped $LiFe_{1-x}V_xAs$ single crystals. The superconducting transition temperature T_c of LiFeAs decreases rapidly at a rate of 7 K per 1% V. The Hall coefficient of LiFeAs switches from negative to positive with 4.2% V doping, showing that V doping introduces hole carriers. This observation is further confirmed by the evaluation of the Fermi surface volume measured by angle-resolved photoemission spectroscopy (ARPES), from which a 0.3 hole doping per V atom introduced is deduced. Interestingly, the introduction of holes does not follow a rigid band shift. We also show that the temperature evolution of the electrical resistivity as a function of doping is consistent with a crossover from a Fermi liquid to a non-Fermi liquid. Our ARPES data indicate that the non-Fermi liquid behavior is mostly enhanced when one of the hole d_{xz}/d_{yz} Fermi surfaces is well nested by the antiferromagnetic wave vector to the inner electron Fermi surface pocket with the d_{xy} orbital character. The magnetic susceptibility of $LiFe_{1-x}V_xAs$ suggests the presence of strong magnetic impurities following V doping, thus providing a natural explanation to the rapid suppression of superconductivity upon V doping.

I. INTRODUCTION

The Fe-based superconductors are multiband systems with a Fermi surface (FS) composed of several pockets with different orbital characters [1]. The complexity of the FS allows different low-energy scattering processes that can stabilize long-range magnetic order and that have even been proposed to induce superconducting (SC) pairing in these compounds [2–4]. A recent report on Co-doped LiFeAs reveals a direct correlation between FS nesting and manifestations of non-Fermi liquid (NFL) behavior in the absence of a clear quantum critical point [5], i.e., a phase transition at zero temperature. Indeed, the largest deviation of the temperature exponent in the power law used to fit the temperature dependence of the electrical resistivity is found for a doping corresponding to a good nesting of the largest hole FS pocket with d_{xy} character with the electron pockets. Unfortunately, whether the relevant scattering causing the NFL behavior is orbital dependent is unclear. A natural way to settle this issue is to hole-dope LiFeAs and search for similar scattering but with FS pockets carrying different orbital characters. Although attempts to hole-dope the $BaFe_2As_2$ system by substituting Fe by lighter 3d elements have been done using Mn [6–9] and Cr [10–14], the literature lacks a similar study on LiFeAs, and in either cases V has not been used to induce hole doping.

In this paper we report the synthesis and characterization of V-doped LiFeAs. The SC transition temperature T_c of LiFeAs is dramatically suppressed by V doping at a rate of 7 K per 1% V, which is much faster than for Co/Ni/Cu doping. Our Hall coefficient R_H and angle-resolved photoemission spectroscopy

(ARPES) measurements indicate that each V dopant releases 0.3 hole carrier. With the V doping level increasing, we observe a crossover from Fermi liquid (FL) to non-FL to FL behavior, which we explain by increased interorbital scattering mediated by low-energy spin fluctuations when a good nesting is found between the inner d_{xy} electron FS pocket at the M point and the outer d_{xz}/d_{yz} hole FS pocket at the Γ point. Also, our susceptibility measurements suggest that V doping gives rise to magnetic impurities, thus providing a simple explanation for the rapid suppression of T_c upon V doping.

II. EXPERIMENT

The single crystals of $LiFe_{1-x}V_xAs$ used in this study have been synthesized using the self-flux method and the details can be found elsewhere [15]. Li_3As and $Fe_{1-x}V_xAs$ were first synthesized as precursors by a solid state reaction method. To synthesize Li_3As, Li lump and As powder were sealed into a Ti tube under 1 atm Ar and sintered at 650 °C for 10 h. $Fe_{1-x}V_xAs$ was obtained by mixing Fe, V, and As powders, pressing the mixture into pieces and heating them at 700 °C for 15 h in an evacuated quartz tube. We then mixed Li_3As, $Fe_{1-x}V_xAs$, and As together with the ratio of $Li_3As:Fe_{1-x}V_xAs:As = 1:0.9:1.1$, and put the mixture into an alumina crucible, sealed it into a Nb tube under 1 atm Ar atmosphere, and sealed that into a quartz tube. The mixture was first heated to 1100 °C for 50 h and then slowly cooled down to 750 °C at the rate of 2 °C/h to grow the single crystals. The chemical compositions of the $LiFe_{1-x}V_xAs$ single crystals used hereafter were determined by energy dispersive x-ray spectroscopy (EDX) with an experimental accuracy of about 10%.

The samples were characterized by x-ray powder diffraction (XRD) in the 10°–80° range using a Philips X'pert diffractometer at a scanning rate of 10° per minute. The dc magnetic susceptibility was measured by using a vibrating

---

*[*]p.richard@iphy.ac.cn
[†]wangxiancheng@iphy.ac.cn
[‡]dingh@iphy.ac.cn
[§]cqjin@iphy.ac.cn

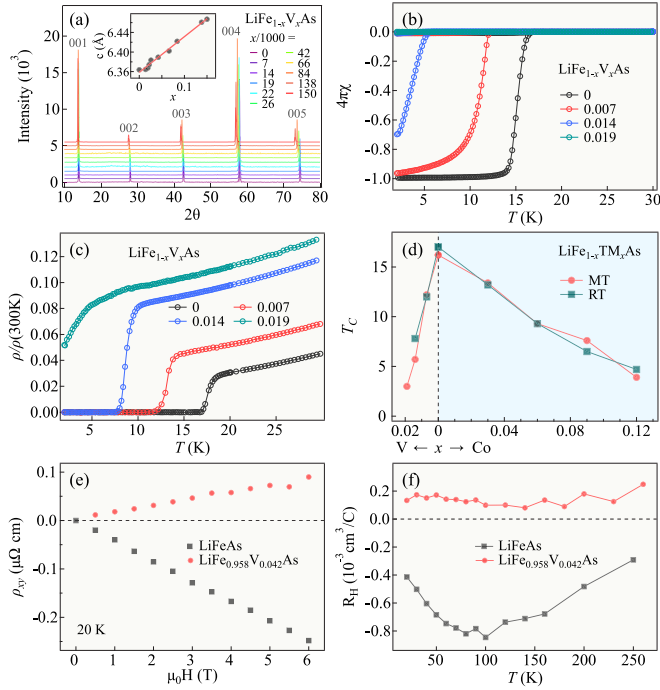FIG. 1. (a) XRD patterns of $LiFe_{1-x}V_xAs$ single crystals. The inset shows the dependence of the lattice constant c versus the doping level x, fit to a linear line (red). (b) and (c) Temperature dependence of the magnetic susceptibility and the normalized resistivity $\rho/\rho(300\,K)$ of $LiFe_{1-x}V_xAs$ single crystals. (d) Evolution of T_c as a function of V and Co doping in $LiFe_{1-x}TM_xAs$ (TM = V and Co) single crystals. MT and RT represent T_c determined from the magnetic susceptibility and from the resistivity, respectively. The data for $LiFe_{1-x}Co_xAs$ are extracted from Ref. [15], copyright ©2014 by IOP Publishing. (e) Magnetic field dependence of the Hall resistivity ρ_{xy} of LiFeAs and $LiFe_{0.958}V_{0.042}As$ single crystals at 20 K. (f) Temperature dependence of the Hall coefficient R_H of LiFeAs and $LiFe_{0.958}V_{0.042}As$ single crystals.

sample magnetometer (VSM) with a magnetic field of 30 Oe for characterizing the superconducting transition, and of 1 T for studying the effective magnetic moment. Resistivity and Hall coefficient measurements were performed using a six-probe technique on a Quantum Design instrument physical property measurement system (PPMS) with a magnetic field up to 6 T. We performed ARPES measurements at the Dreamline beamline of the Shanghai Synchrotron Radiation Facility and at the I05 beamline of the Diamond Light Source using Scienta D80 and Scienta R4000 analyzers, respectively. The energy and angular resolutions have been set to 10 meV and 0.2°, respectively. All measurements have been recorded at 20 K with 51 eV photons (vertical momentum $k_z \approx 0$ [16]) in s and p polarization configurations.

III. RESULTS AND DISCUSSION

Figure 1(a) shows the XRD patterns of $LiFe_{1-x}V_xAs$ single crystals. Only 00l peaks are observed and the full width at half maxima are smaller than 0.2°, suggesting high single crystal quality. The inset shows the doping evolution of the c axis, which is consistent with Vegard's law. While

superconductivity in most Fe-based superconductors occurs upon carrier doping, a T_c of 18 K is observed in pristine LiFeAs [17,18]. The T_c of LiFeAs decreases linearly upon electron doping with Co, Ni, or Cu [15,19]. Figures 1(b) and 1(c) show the temperature dependence of the magnetic susceptibility and the resistivity for $LiFe_{1-x}V_xAs$ with $x <$ 0.019. All $LiFe_{1-x}V_xAs$ samples with $x < 0.019$ exhibit diamagnetic susceptibility and SC zero resistivity. The SC transition T_c decreases from 16 K to 6 K with x increasing to 0.014. Superconductivity disappears at $x = 0.019$, as shown in Fig. 1(c). As displayed in Fig. 1(d), T_c decreases almost linearly with V doping at a rate of 7 K per 1%V, which is much faster than for electron doping with Co/Ni/Cu [20,21]. Indeed, 1% doping with Co and Ni in the $LiFe_{1-x}(Co/Ni)_xAs$ system suppresses T_c by 1 and 2.2 K, respectively. Cu doping suppresses T_c at a rate similar as Ni doping but the FS almost does not change. It was proposed that the suppression of T_c by Cu dopant is mainly due to its strong impurity scattering effect [15].

We further study the effect of V doping in the LiFeAs system from Hall resistivity measurements. Figure 1(e) compares the Hall resistivity ρ_{xy} of LiFeAs and $LiFe_{0.958}V_{0.042}As$ versus the applied magnetic field measured at 20 K. In contrast to LiFeAs, for which the slope of $d\rho_{xy}/dH$ is negative, the slope of $d\rho_{xy}/dH$ is positive for $LiFe_{0.958}V_{0.042}As$, suggesting that the substitution of Fe by V dopes the system with holes. The temperature dependence of the Hall coefficient R_H for these samples is shown in Fig. 1(f). For LiFeAs, R_H is negative with a minimum value at about 100 K, which is consistent with a previous work [22]. However, for the $LiFe_{0.958}V_{0.042}As$ sample, R_H is positive with a smaller temperature dependence within the measured temperature range. This sign reversal of R_H is an explicit indication of hole doping with the introduction of V.

In order to confirm and quantify the introduction of hole carriers in the V-doped LiFeAs samples, we recorded ARPES data at selected sample dopings. We show in Figs. 2(a)–2(d) the FS measured for the V doping levels $x = 0, 0.042, 0.066$, and 0.084, respectively. For each sample, hole FS pockets at Γ and electron FS pockets at M are observed, as indicated by the red contours extracted from the ARPES intensity maps. The FS topology is typical of that of most iron pnictides [1]. We note that the band structure of highly V-doped samples ($x = 0.066, 0.084$), and in particular the β FS sheet (d_{xy} character), is not as sharp as that of pristine LiFeAs. This is intrinsically due to strong impurity scattering. The FS can be well approximated nevertheless, especially from the trend observed in the doping evolution at low doping, where the bands are clearly identifiable. Surprisingly, we find that while the α (not crossing the Fermi level E_F in LiFeAs) and α' FS pockets get enlarged with the V concentration increasing, the other FSs barely change with doping. Consequently, we use the FSs extracted in LiFeAs to approximate the β FS pocket and the electronlike pockets. Obviously, these FS contours are consistent with the FS intensity patterns at all dopings, thus validating our approximation. As shown in Figs. 2(e) and 2(f), error bars are used to account for our limited accuracy in determining the FSs precisely at high doping.

According to the Luttinger theorem, the electronic carrier concentration is determined by the algebraic sum of all the
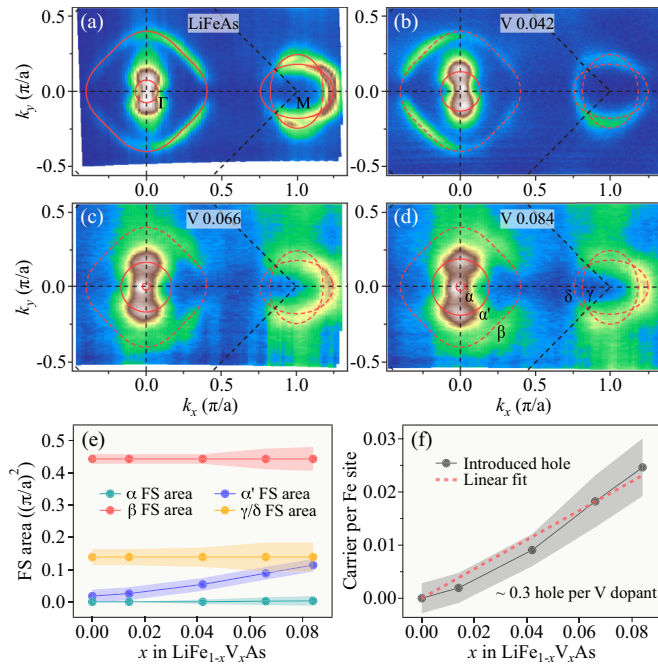
FIG. 2. (a)–(d) ARPES FS intensity maps of LiFe$_{1-x}$V$_x$As for $x = 0$, 0.042, 0.066, and 0.084, respectively. The maps were recorded with s polarized 51 eV photons and integrated within a 10 meV energy window centered at E_F. The solid red lines appended on the plots are extracted FS contours at each doping. The dashed red lines correspond to data extracted in LiFeAs. (e) Calculated area of different FS pockets as a function of doping. (f) Number of carriers introduced by the Fe $\rightarrow$ V substitution deduced from the FS volume. The dashed pink line is a linear fit showing that a 0.3 hole is added to the system for each V dopant.

FS areas. The calculated area of each FS pocket as a function of doping is shown in Fig. 2(e), and the deduced hole carrier concentration is illustrated in Fig. 2(f). Based on a previous ARPES report [23] exhibiting only small warping of the electronic structure of LiFeAs along the k_z direction, the carrier concentration was evaluated by considering the data recorded in the $k_z = 0$ plane only. As expected from the Hall coefficient data, the substitution of Fe by V leads to hole doping. However, we conclude from a simple linear fit of the introduced free carrier concentration as a function of the V content that only 0.3 hole carrier is introduced per substituting V dopant. We note that neglecting the slight three dimensionality of the FS leads to an uncertainty smaller than 0.05 holes. The experimental doping of 0.3 ± 0.1 is ten times smaller than the "nominal" value, which contrasts with the Co- and Ni-doped cases [5,19]. Co doping into LiFeAs can be approximated by a rigid band shift with one free electron introduced for each Co atom. The electron FS pockets become larger while the hole FS pockets shrink upon Co doping in LiFeAs, with their algebraic sum respecting the Luttinger theorem [5]. The situation is quite different in V-doped LiFeAs. As indicated in Fig. 2(e), the change in the free carrier concentration is practically related only to the α' FS pocket, thus indicating that V doping does not follow a rigid band shift.

This unusual band structure evolution with V doping is further illustrated in Fig. 3. We use s polarized and p polarized
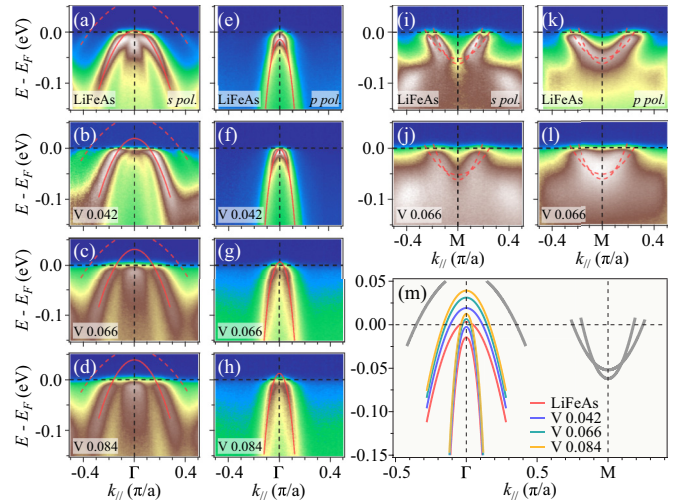

FIG. 3. (a)–(d) ARPES intensity plots near Γ of LiFe$_{1-x}$V$_x$As recorded with s polarized light for $x = 0$, 0.042, 0.066, and 0.084, respectively. (e)–(h) Same as (a)–(d) but recorded with p polarized light. (i),(j) Intensity plots near M for $x = 0$ and 0.066 samples, obtained at 20 K along the Γ-M direction, with s polarized 51 eV photons. (k),(l) Same as (i),(j) but using p polarized photons. (m) Comparison of the band dispersions. The outer holelike band and the electronlike bands, in gray, do not change within the experimental uncertainties.

incident light to highlight the bands carrying different orbital characters. As shown in Figs. 3(a)–3(h), the inner hole bands at Γ (d_{xz}/d_{yz}) shift towards lower binding energy upon V doping, as expected. In contrast, the dispersions of the outer hole band at Γ [d_{xy}, see Figs. 3(a)–3(d)] and of the electron bands at M [Figs. 3(i)–3(l)] are practically unchanged, at least within the current experimental uncertainties. This is summarized in Fig. 3(m). The reason for this dichotomy of band filling behavior in V-doped LiFeAs is unclear and goes beyond the scope of this paper.

A recent report on Co-doped LiFeAs indicates that the improvement upon doping of the nesting conditions between the hole and electron FS pockets leads to a FL to a NFL behavior [5]. As the size of the α' FS pocket increases with V doping, whereas the electron FS pockets remain nearly unchanged, one can wonder if FS nesting can also lead to a NFL in this system. To check this scenario, we measured the resistivity of the LiFe$_{1-x}$V$_x$As samples as a function of the temperature T and fitted the data with $\rho = \rho_0 + AT^n$, where A and n are constants and ρ_0 is the residual resistivity (Fig. 4). To minimize contamination from the semiconducting transition at low temperature for highly doped samples, we compare the results obtained with three different temperature ranges. In the first series of fits [fit1 in Fig. 4(g)], the lowest temperature is chosen as low as possible, but with the minimum of the resistivity curve outside of the fitting range. The corresponding temperature range fits are given by the red curves in Figs. 4(b)–4(f). In the second series [fit2 in Fig. 4(g)], the fit starts at the semiconducting transition. Finally, for the last series of fit [fit3 in Fig. 4(g)], the resistivity was fitted in the 30–70 K temperature range for all dopings. Despite small discrepancies, the doping evolution of the exponent n, displayed in Fig. 4(g), has the same trends for all the fitting methods.
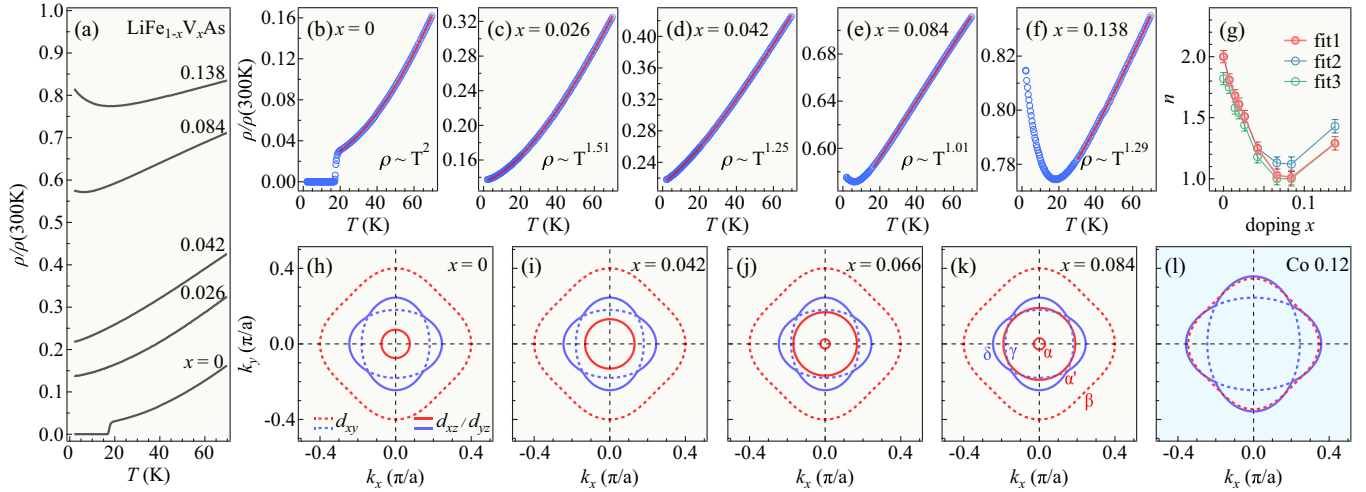
FIG. 4. (a) Temperature dependence of the normalized resistivity $\rho/\rho(300\text{ K})$ for five selected $\text{LiFe}_{1-x}\text{V}_x\text{As}$ single crystals. (b)–(f) Same as (a) both with a zoom on each resistivity curve. For each sample, $\rho/\rho(300\text{ K})$ is fitted using $\rho = \rho_0 + AT^n$. (g) Exponent n as a function of x. The red circles (fit1) represent n values obtained from the fitted curves shown in Figs. 3(b)–3(f). The cyan circles (fit2) are the values obtained in the temperature range that starts by the metal-insulator transition or T_c. The green circles (fit3) are the values obtained in the 30–70 K temperature range. (h)–(k) Evolution of the hole FSs (red) and electron FSs (blue) as a function of x in $\text{LiFe}_{1-x}\text{V}_x\text{As}$. The electron FSs pockets have been shifted to the Γ point for a better comparison. The electronlike pockets and the large β holelike pocket are treated as doping independent, in agreement with the experimental results. (l) Same as (h)–(k) but for $\text{LiFe}_{0.88}\text{Co}_{0.12}\text{As}$ (extracted from Ref. [5]), which shows the most pronounced NFL behavior in the $\text{LiFe}_{1-x}\text{Co}_x\text{As}$ series.

As with Co-doped LiFeAs [5], the exponent n deviates from 2 with the introduction of V dopants, suggesting a NFL regime. We emphasize that this is already true at low doping, away from the semiconducting transition. Interestingly, n reaches a minimum of 1.01 for a doping of $x = 0.084$, before increasing again towards 2 with further doping. We caution that although the precise values of the exponent n are questionable at high doping, the trend is clear. As with Co-doped LiFeAs, this behavior strongly suggests that V-doped LiFeAs is host to low-energy fluctuations enhanced with the nesting conditions. The observation of a NFL behavior without quantum critical point in both Co-doped and V-doped LiFeAs is consistent with a recent theoretical study emphasizing the impact of nesting on the temperature evolution of the electrical conductivity [24]. We caution though that the linear resistivity in the cuprates was previously derived in the context of a FL with a large density of states (like a van Hove singularity) near E_F [25,26], a condition that also applies to Fe-based superconductors near good nesting conditions.

As shown in Fig. 4(k), a good nesting is found at $x = 0.084$ between the α' FS pocket, which carries a d_{xz}/d_{yz} orbital character, and the inner electron FS pocket γ, mainly derived from the d_{xy} orbital. This situation is symmetrical to the one found in Co-doped LiFeAs, for which the lowest n coincides with the best nesting conditions between the outer hole FS pocket β with a d_{xy} orbital character and the outer electron FS pocket δ, which carries a dominant d_{xz}/d_{yz} orbital character [Fig. 4(l)]. It is thus fair to say that the NFL behavior is mainly due to low-energy interorbital scattering with the scattering vector $\mathbf{Q}$ corresponding to the wave vector between Γ and M. Such experimental observation is consistent with theoretical calculations indicating that the coupling to the wave vector $\mathbf{Q}$ is favored between different orbital states [27]. We caution that unlike the assumption made

in Ref. [27], this scattering is not obviously correlated to the SC pairing.

However, our data suggest that the magnetic properties of $\text{LiFe}_{1-x}\text{V}_x\text{As}$ go beyond simple FS nesting. When $x > 0.066$, $\text{LiFe}_{1-x}\text{V}_x\text{As}$ displays a semiconducting behavior at low temperature similar to the one observed in Cu-doped Fe-based superconductors. A weak semiconducting behavior emerges at $x \sim 0.13$ for $\text{LiFe}_{1-x}\text{Cu}_x\text{As}$ [28] and at $x \sim 0.033$ for $\text{NaFe}_{1-x}\text{Cu}_x\text{As}$ [21]. A crossover from metallic to semiconducting behavior with Cu doping has also been observed in $\text{Ba}(\text{Fe}_{1-x}\text{Cu}_x)_2\text{As}_2$ [29], $\text{Sr}(\text{Fe}_{1-x}\text{Cu}_x)_2\text{As}_2$ [30], and $\text{Fe}_{1.01-x}\text{Cu}_x\text{Se}$ [31], and it was proposed that Cu dopants in these materials behave like strong scatterers inducing a metal-insulator transition due to Anderson localization [32]. Since the critical doping for the metal-semiconductor crossover is even lower in $\text{LiFe}_{1-x}\text{V}_x\text{As}$, i.e., $x = 0.066$ in $\text{LiFe}_{1-x}\text{V}_x\text{As}$ as compared with $x = 0.4$ in $\text{LiFe}_{1-x}\text{Co}_x\text{As}$ and $x = 0.13$ in $\text{LiFe}_{1-x}\text{Cu}_x\text{As}$, we also assume that the V impurities are strong scattering centers.

We also measured the magnetic susceptibility under magnetic field up to 1 T. The amplitude of the magnetic susceptibility in $\text{LiFe}_{1-x}\text{V}_x\text{As}$ [Fig. 5(a)] is about one order of magnitude higher than for $\text{LiFe}_{1-x}\text{Co}_x\text{As}$ [Fig. 5(b)] and $\text{LiFe}_{1-x}\text{Cu}_x\text{As}$ [Fig. 5(c)]. As shown in Figs. 5(d) and 5(e), respectively, the susceptibilities of LiFeAs and $\text{LiFe}_{0.85}\text{V}_{0.15}\text{As}$ follow the Curie-Weiss law $1/(\chi - \chi_0) = (T - \theta)/C$ at low temperature, where θ is the Curie temperature. The Curie-Weiss law allows us to extract an effective magnetic moment μ_{eff}. The results as a function of the content x, displayed in Fig. 5(f), indicate that while μ_{eff} varies only slightly upon Co and Cu doping, it is greatly enhanced with V doping.

The enhancement of μ_{eff} by Mn dopants has been reported in the NaFeAs system [33], where 4%-Mn dopants increase the effective moment of $\text{Na}(\text{Fe}_{0.97-x}\text{Co}_{0.03}\text{Mn}_x)\text{As}$
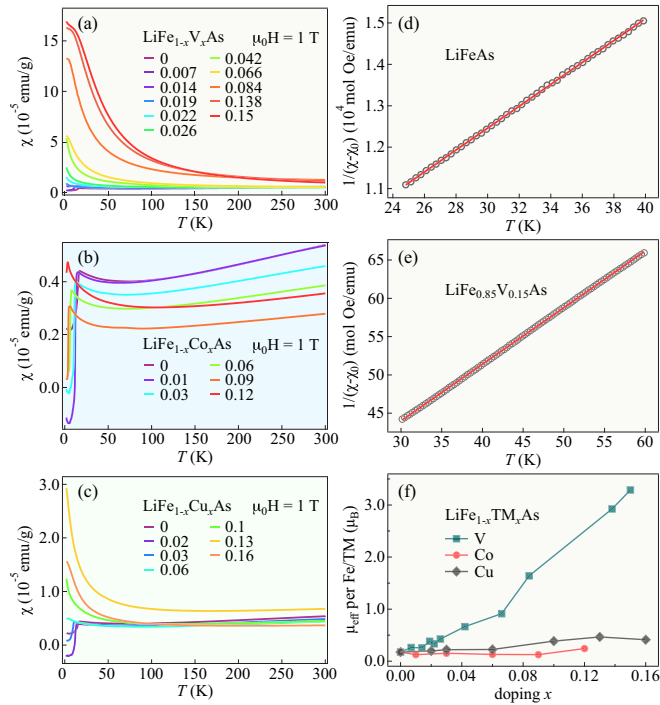
FIG. 5. Temperature dependence of the magnetic susceptibility in a 1 T magnetic field of (a) $LiFe_{1-x}V_xAs$, (b) $LiFe_{1-x}Co_xAs$, and (c) $LiFe_{1-x}Cu_xAs$ single crystals. (d) and (e) Magnetic susceptibility fitted according to the Curie-Weiss law $1/(\chi - \chi_0) = (T - \theta)/C$. (f) Effective moment per Fe/TM site as a function of the doping concentration x for $LiFe_{1-x}TM_xAs$ (TM = V, Co, and Cu) single crystals.

from about 0.4 to 1.8 μ_B per Fe/Co/Mn site. The Mn dopants in $Na(Fe_{0.97-x}Co_{0.03}Mn_x)As$ are considered to be magnetic impurities, and the spectroscopic signature of Kondo screening on the Mn adatoms has been observed by scanning tunneling spectroscopy [33,34]. Accordingly, although our experiment does not allow us to conclude unambiguously that the magnetic moments develop on the V sites, we speculate that the V dopants in our study are magnetic impurities because of the enhancement of μ_{eff} with V substitution.

The effective magnetic moment of LiFeAs is enhanced to about 3.3 μ_B by 16% V dopants, which is unexpectedly higher than for usual Fe-based superconductors. Yet, an even higher effective magnetic moment of about $4\mu_B$ has been reported in $Fe_{1+x}Te$ and explained by a Kondo-type behavior (i.e., with local magnetic moments entangled with itinerant electrons) [35–37]. Similarly, V dopants are likely to give rise to magnetic impurities and induce entanglement between the local magnetic moments and the itinerant electrons. Here the local magnetic moments may come from either magnetic impurities or from Fe, but further discussion is beyond the scope of this paper. Finally, we note that the observation of strong magnetic moments offers one possible explanation to the rapid suppression of T_c in $LiFe_{1-x}V_xAs$.

IV. SUMMARY

In summary, we synthesized and characterized single crystals of $LiFe_{1-x}V_xAs$. Using Hall coefficient and ARPES measurements, we showed that the substitution of Fe by V dopes the system with holes at a rate of 0.3 hole/V. We showed from the temperature dependence of the resistivity data that the system exhibits a NFL behavior that is enhanced around doping where our ARPES measurements indicate a good FS nesting between FS pockets carrying different orbital characters, suggesting that the NFL behavior is induced by low-energy interorbital scattering by the antiferromagnetic wave vector. Finally, the magnetic susceptibility of $LiFe_{1-x}V_xAs$ suggests that strong magnetic moments develop following V doping, thus providing a natural explanation for the rapid suppression of superconductivity found upon doping.

[1] P. Richard, T. Sato, K. Nakayama, T. Takahashi, and H. Ding, Rep. Prog. Phys. **74**, 124512 (2011).

[2] I. I. Mazin, D. J. Singh, M. D. Johannes, and M. H. Du, Phys. Rev. Lett. **101**, 057003 (2008).

[3] H. Ding, P. Richard, K. Nakayama, K. Sugawara, T. Arakane, Y. Sekiba, A. Takayama, S. Souma, T. Sato, T. Takahashi, Z. Wang, X. Dai, Z. Fang, G. F. Chen, J. L. Luo, and N. L. Wang, Europhys. Lett. **83**, 47001 (2008).

[4] S. Graser, T. A. Maier, P. J. Hirschfeld, and D. J. Scalapino, New J. Phys. **11**, 025016 (2009).

[5] Y. M. Dai, H. Miao, L. Y. Xing, X. C. Wang, P. S. Wang, H. Xiao, T. Qian, P. Richard, X. G. Qiu, W. Yu, C. Q. Jin, Z. Wang, P. D. Johnson, C. C. Homes, and H. Ding, Phys. Rev. X **5**, 031035 (2015).

[6] Y. Liu, D. L. Sun, J. T. Park, and C. T. Lin, Physica C **470**, S513 (2010).

[7] M. G. Kim, A. Kreyssig, A. Thaler, D. K. Pratt, W. Tian, J. L. Zarestky, M. A. Green, S. L. Bud'ko, P. C. Canfield, R. J. McQueeney, and A. I. Goldman, Phys. Rev. B **82**, 220503(R) (2010).

[8] A. Thaler, H. Hodovanets, M. S. Torikachvili, S. Ran, A. Kracher, W. Straszheim, J. Q. Yan, E. Mun, and P. C. Canfield, Phys. Rev. B **84**, 144528 (2011).

[9] A. Pandey, V. K. Anand, and D. C. Johnston, Phys. Rev. B **84**, 014405 (2011).

[10] A. S. Sefat, D. J. Singh, L. H. VanBebber, Y. Mozharivskyj, M. A. McGuire, R. Jin, B. C. Sales, V. Keppens, and D. Mandrus, Phys. Rev. B **79**, 224524 (2009).

[11] S. L. Bud'ko, S. Nandi, N. Ni, A. Thaler, A. Kreyssig, A. Kracher, J.-Q. Yan, A. I. Goldman, and P. C. Canfield, Phys. Rev. B **80**, 014522 (2009).

[12] E. Colombier, M. S. Torikachvili, N. Ni, A. Thaler, S. L. Bud'ko, and P. C. Canfield, Supercond. Sci. Technol. **23**, 054003 (2010).

[13] K. Marty, A. D. Christianson, C. H. Wang, M. Matsuda, H. Cao, L. H. VanBebber, J. L. Zarestky, D. J. Singh, A. S. Sefat, and M. D. Lumsden, Phys. Rev. B **83**, 060509(R) (2011).

[14] J. P. Clancy, B. D. Gaulin, and A. S. Sefat, Phys. Rev. B **85**, 054115 (2012).

[15] L. Y. Xing, H. Miao, X. C. Wang, J. Ma, Q. Q. Liu, Z. Deng, H. Ding, and C. Q. Jin, J. Phys.: Condens. Matter **26**, 435703 (2014).

[16] H. Miao, T. Qian, X. Shi, P. Richard, T. K. Kim, M. Hoesch, L. Y. Xing, X.-C. Wang, C.-Q. Jin, J.-P. Hu, and H. Ding, Nat. Commun. **6**, 6056 (2015).

[17] X. C. Wang, Q. Q. Liu, Y. X. Lv, W. B. Gao, L. X. Yang, R. C. Yu, F. Y. Li, and C. Q. Jin, Solid Stat. Commun. **148**, 538 (2008).

[18] J. H. Tapp, Z. Tang, B. Lv, K. Sasmal, B. Lorenz, P. C. W. Chu, and A. M. Guloy, Phys. Rev. B **78**, 060505(R) (2008).

[19] M. J. Pitcher, T. Lancaster, J. D. Wright, I. Franke, A. J. Steele, P. J. Baker, F. L. Pratt, W. T. Thomas, D. R. Parker, S. J. Blundell, and S. J. Clarke, J. Am. Chem. Soc. **132**, 10467 (2010).

[20] P. C. Canfield, S. L. Bud'ko, N. Ni, J. Q. Yan, and A. Kracher, Phys. Rev. B **80**, 060501 (2009).

[21] A. F. Wang, J. J. Lin, P. Cheng, G. J. Ye, F. Chen, J. Q. Ma, X. F. Lu, B. Lei, X. G. Luo, and X. H. Chen, Phys. Rev. B **88**, 094516 (2013).

[22] O. Heyer, T. Lorenz, V. B. Zabolotnyy, D. V. Evtushinsky, S. V. Borisenko, I. Morozov, L. Harnagea, S. Wurmehl, C. Hess, and B. Büchner, Phys. Rev. B **84**, 064512 (2011).

[23] V. Brouet, D. LeBoeuf, P.-H. Lin, J. Mansart, A. Taleb-Ibrahimi, P. Le Fèvre, F. Bertran, A. Forget, and D. Colson, Phys. Rev. B **93**, 085137 (2016).

[24] C. Setty and P. W. Phillips, Phys. Rev. B **93**, 094516 (2016).

[25] G. Kastrinakis, Physica C **340**, 119 (2000).

[26] G. Kastrinakis, Phys. Rev. B **71**, 014520 (2005).

[27] J. Zhang, R. Sknepnek, R. M. Fernandes, and J. Schmalian, Phys. Rev. B **79**, 220502(R) (2009).

[28] L. Y. Xing, X. C. Wang, Z. Deng, S. J. Zhang, S. M. Feng, W. M. Li, Q. Q. Liu, and C. Q. Jin, Int. J. Mod. Phys. B **29**, 1542023 (2015).

[29] N. Ni, A. Thaler, J. Q. Yan, A. Kracher, E. Colombier, S. L. Bud'ko, P. C. Canfield, and S. T. Hannahs, Phys. Rev. B **82**, 024519 (2010).

[30] Y. J. Yan, P. Cheng, J. J. Ying, X. G. Luo, F. Chen, H. Y. Zou, A. F. Wang, G. J. Ye, Z. J. Xiang, J. Q. Ma, and X. H. Chen, Phys. Rev. B **87**, 075105 (2013).

[31] A. J. Williams, T. M. McQueen, V. Ksenofontov, C. Felser, and R. J. Cava, J. Phys.: Condens. Matter **21**, 305701 (2009).

[32] S. Chadov, D. Schärf, G. H. Fecher, C. Felser, L. Zhang, and D. J. Singh, Phys. Rev. B **81**, 104523 (2010).

[33] Q. Deng, X. Ding, S. Li, J. Tao, H. Yang, and H.-H. Wen, New J. Phys. **16**, 063020 (2014).

[34] Z. Wang, D. Fang, Q. Deng, H. Yang, C. Ren, and H.-H. Wen, Phys. Rev. B **89**, 214515 (2014).

[35] I. A. Zaliznyak, Z. Xu, J. M. Tranquada, G. Gu, A. M. Tsvelik, and M. B. Stone, Phys. Rev. Lett. **107**, 216403 (2011).

[36] R. Hu, E. S. Bozin, J. B. Warren, and C. Petrovic, Phys. Rev. B **80**, 214514 (2009).

[37] C. Koz, S. Rößler, A. A. Tsirlin, C. Zor, G. Armağan, S. Wirth, and U. Schwarz, Phys. Rev. B **93**, 024504 (2016).